Journal of Renewable Energies

Revue des Energies Renouvelables

Journal home page : https://revue.cder.dz/index.php/rer

Research paper

Experimental Study on Enhancing Lead Oxide Photoelectrochemical Efficiency with Tin Substrate Modifications for Renewable Energy Systems.

Tawfiq Dilmi[a,b,1], Achour Dakhouche[b], H'mida Latelli[c], Ahmed Saoudi[d]

[a]*Mira Abderahman University, Faculty of Sciences exact, Department of Physics, 06000 Bejaia, Algeria*
[b]*Inorganic Materials Laboratory, Department of Chemistry, Faculty of Sciences, Mohamed Boudiaf University, M'sila, Algeria.*
[c]*Department of Physics, Faculty of Sciences, Mohamed Boudiaf University, M'sila, Algeria.*
[d] *Laboratory: Cites, Environment, Society and Sustainable Developent (CESSD), M'sila 28000, Algeria*

ARTICLEINFO

Articlehistory:
Received January 4, 2024
Accepted October 20, 2024

Keywords:
Pb-Sn alloy,
Lead Oxide,
corrosion,
Renewable Energy,
semiconductor

ABSTRACT

This work focuses on the photoelectrochemical and semicondictrise study of the corrosion layer formed in the dark on Lead and lead-tin alloys in a 0.5M sulfuric acid solution: Electrochemical Impedance Spectroscopy (EIS), Linear Sweeping Voltage (LSV), Mott-Schottky plots and photocurrent measurements. The composition was determined respectively by XRD diffraction and SEM electron microscopy. The findings indicate that the incorporation of tin leads to a reduction in the corrosion layer thickness while significantly enhancing its electrical conductivity. This effect is attributed to the formation of conductive, non-photoactive tin oxides and the development of a compact interfacial the layer separating the grid from the positive active material.

1. INTRODUCTION

Since the early 19th century, scientists and researchers have explored various types of semiconductors, driven by their remarkable industrial properties and diverse range of applications. In recent decades, their interest has increased further due to their penetration in most of the industries that form the backbone of the world's economic and commercial life. Due to its unique properties and wide range of applications, lead oxide (PbO) has been the subject of extensive research as a semiconductor. PbO is commonly utilized in

[1]*Corresponding author, Tawfiq Dilmi: dilmi2826@gmail.com*
Tel :+ 213 659394147

battery production(Liu et al., 2017), gas sensors (Srivastava & al., 2011), solarcells(D B Patel and I Mukhopadhyay, 2015), optical X-ray detectors(Cimek& al, 2017 ;Mohamed E & al, 2018 ;(El-Mallawany et al., 2018 ;G. Zentai & al, 2013 ;Semeniuk & al, 2017), radiation shieldingmaterials (Mohamed E & al, 2018 ;El-Mallawany et al., 2018), photonics (Cimek & al, 2017 ; Zheng & al, 2014), photocatalytic applications (Liu Shao‐you & al, 2018) and many others by incorporating traces of grafting atoms. Proposal to use lead oxides as compounds abundant on earth for photovoltaics(Ranjbar, 2017 ;Zhuravlev & Korabel'nikov, 2017).

The effect of tin addition on grid passivation has been studied. Tin removes the transition from Pb to α-PbO according to Giess (D. Pavlov, E. Bashtavelova, 1984). Pavlov et al. (Pavlov & Al, 1969) obtained related results, The integration of Sn into the PbO/PbOx crystal lattice is suggested. In research by Takahashi et al. (Pendry, 1999), Tin promotes the growth of α-PbO_2, thereby inhibiting the development of a lead sulfate layer on the grid surface. However, Carter et al. (B.J. Carter, S.D. Stefano, 1986)found that Pb-Ca-Sn anode alloys lose 20% of their original capacity after undergoing 50 deep discharge cycles. Attributed to the high rate of substance forming at the surface, the observed reduction in capacity is due to the lack of interaction between the grid and the active material. Nelson and Wisdom (Nelson & Wisdom, 1991)found that the incorporation of tin during a shallow discharge contributes to the formation of discontinuous oxide films on the grids. The authors also observed that Pb-Sn alloys at the grid/electrolyte interface exhibit intensified corrosive attack along the grain boundaries.

At a buffer charging regime of the battery with Pb-Ca-Sn plates, Weiniger and Siwek (Weininger & Siwek, 1976) did not notice any concentration of $PbSO_4$ around the Pb-Ca-Sn grid. The authors confirmed that tin slows down the reduction of the corrosion layer. Using electrochemical techniques and metallographic research, Rocca et al.(Rocca & Steinmetz, 1999) It has been reported that to prevent the formation of an electrical barrier on the grid surface, the concentration of Sn must be carefully controlled. The researchers only grouped the Pb-Sn alloys into three distinct courses according to their Sn content.

There are many previous studies that have dealt with the subject of the photoelectrochemical properties of lead oxide and have dealt with it from various, including: The study of Pavlov and al, aged (Pavlov & al, 1977 ;Pavlov, 1978 ;Pavlov, 1981), who concluded that when an electrode is illuminated, it has three types of photo-electrochemical processes and a high optical response to the negative film on Pb in H_2SO_4, which goes back to the PbO_x stage according to(R.G. BARRADAS & al, 1981). Barradas and al (Peter, 1983) have experimented with anodic oxidation of lead in H_2SO_4 under the influence of visible white light at different wavelengths, the most prominent of which was that repeated illumination leads to an increase in the light current, but the light sensitivity threshold remains unchanged. Buchanan and Peter(Bullock et al., 1983) also demonstrated by optical current spectroscopy that lead oxide is quadrangular. The results of Kathryn and al. (Buchanan & Peter, 1988)when using pomegranate spectroscopy indicated that lead oxide was formed above the valence PbO_x. The results of the photocurrent by researchers Campbell and Peter (Campbell & Peter, 1991) indicate that the deposited αPbO film is In ethanoate solution it leads to tetrahedral precipitation of PbO within the oxide pores.

Our study builds on these findings by examining how tin substrate modifications enhance PbO's photoelectrochemical efficiency in energy systems. Unlike prior work, we specifically address the role of tin in reducing the thickness of the corrosion layer and improving the photocurrent response under light exposure. This study provides new insights into PbO's application in photoelectrochemical cells (PECs) and lead-acid batteries for renewable energy storage, focusing on the effects of varying tin content (0.2% and 2% Sn) on these properties.

By advancing the understanding of PbO's electrochemical stability, light absorption, and charge separation efficiency, our work contributes to the development of more efficient energy storage and conversion devices within the renewable energy sector.

The findings of this study carry important implications for renewable energy technologies, especially in relation to energy storage and conversion systems. Lead-acid batteries, which are widely used for energy storage in solar and wind power systems, can benefit from the findings of this study. Enhancing the efficiency and durability of PbO-based anodes through tin substrate modifications can lead to improved battery performance, making them more suitable for large-scale renewable energy applications.

Additionally, the enhanced photoelectrochemical properties of PbO demonstrated in this study open up new possibilities for its use in photoelectrochemical cells (PECs), which are critical components in solar fuel generation and water-splitting technologies. PECs convert sunlight into chemical energy by driving reactions such as splitting water into hydrogen and oxygen. By optimizing the PbO substrate composition, we can improve the efficiency of these devices, contributing to the development of sustainable hydrogen production systems.

These findings highlight the broader impact of PbO in renewable energy technologies, from efficient energy storage in lead-acid batteries to advanced solar cells and hydrogen generation technologies.

The objective of this study is to elucidate the influence of the substrate on the photoelectrochemical and semiconductive properties of lead oxide in a 0.5 M H_2SO_4 solution, employing various analytical techniques.

2. EXPERIMENTAL

2.1 Alloy preparation (Pb-Sn)

Lead and 99.98% pure tin were used in the experiments to produce samples. For the preparation of the following alloys, sufficient quantities of Pb and Sn were weighed (0.2 % and 2 % Sn). The melting of the weighed masses was carried out in a porcelain crucible which was placed in a furnace as shown in Fig. 1 (a). When the temperature was about 340 °C (above the lead melting temperature of 237 °C), the crucible was then removed from the furnace and its contents were poured into a cylindrical steel mold with a diameter of 1 cm as shown in Fig. 1 (b). When the mould was discarded, the cylindrical steel was removed from the mould.

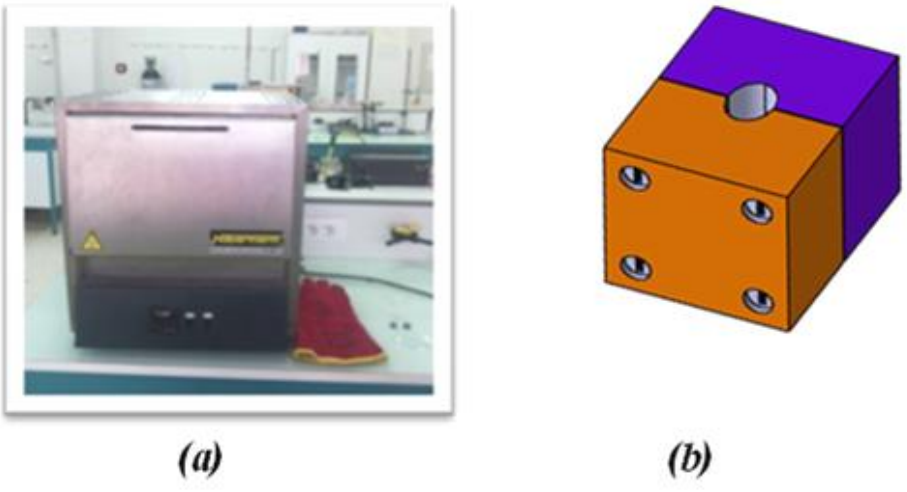

Fig. 1. (a) Muffle furnace (b) Mold used for making alloys.

2.2 Mechanical preparation

An abrasive paper with a grit size ranging from 800 to 4000 was utilized in this process to eliminate surface impurities and achieve a smooth finish. Following the polishing step, the specimens were cleaned with acetone to remove grease, rinsed thoroughly with distilled water, and rapidly dried with a dryer.

2.3 Electrochemical cell

It should be noted that the electrochemical experiments were carried out in a commercial electrochemical corrosion cell (Fig. 2) which was built in the laboratory using Teflon. The description of the cell shows that it is cubic in shape. It was produced by PVC-type plates. Moreover, it was observed that the electrode under test lifted by accumulating on a cell wall.

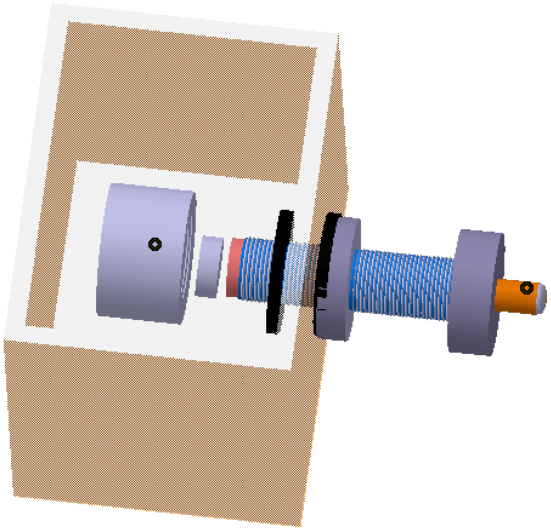

Fig. 2. Electrochemical cell

2.4 Electrodes

In our study, we employed a three-electrode electrochemical cell, with the working electrode being a PbSn alloy sample. The alloy was formed into cylindrical pellets with dimensions of 1 cm in diameter and 0.5 cm in thickness. The working electrode was laterally mounted on one of the cell walls. The counter-electrode consisted of a pure Pb plate shaped into a pellet with a surface area of 2 cm^2, positioned opposite and parallel to the working electrode. A mercury sulfate electrode $Hg/Hg_2SO_4/K_2SO_4$, filled with a saturated potassium sulfate solution, was used as the reference electrode to measure the potential of the working electrode.

2.5 Electrolyte solutions

The electrolyte is a 0.5 M H_2SO_4 solution prepared from a pure solution for SIGMA-ALDRICH analysis with a density of 1.84g / cm^3 and 96% purity using distilled water.

2.6 Principle and equipment

Initially, the electrochemical cell was placed inside a black box, with a potentiostat/galvanostat (AUTOLAB PGSTAT302N) controlled via computer, using NOVA 2.1 software for data acquisition and analysis. Illumination was directed perpendicularly onto the electrode surface, ensuring that no external light entered the system by closing the black box's lid (Fig. 3). Before conducting potentiodynamic experiments, the working electrode's potential was held at the hydrogen evolution potential for 20 minutes to remove surface impurities. Following assembly, the working electrode underwent potentiostatic anodization at 0.7 V with reference to the saturated $Hg/Hg_2SO_4/K_2SO_4$ electrode for 2 hours to develop a lead monoxide layer on the substrate. The working electrode surface was subjected to repeated illuminations with white light for 30-second intervals, with 3-minute dark periods between illuminations. Electrochemical impedance spectroscopy was conducted in potentiostatic mode, covering a frequency range of 100 mHz to 100 kHz with a 10-mV amplitude potential. Tafel plots were generated from linear sweep voltammetry (LSV) data. X-ray

diffraction (XRD) analysis was performed using a Bruker diffractometer (CuKα = 1.54 Å) under a 40-kV voltage, scanning from 2θ = 10° to 70° at a rotation speed of 0.02°/s.

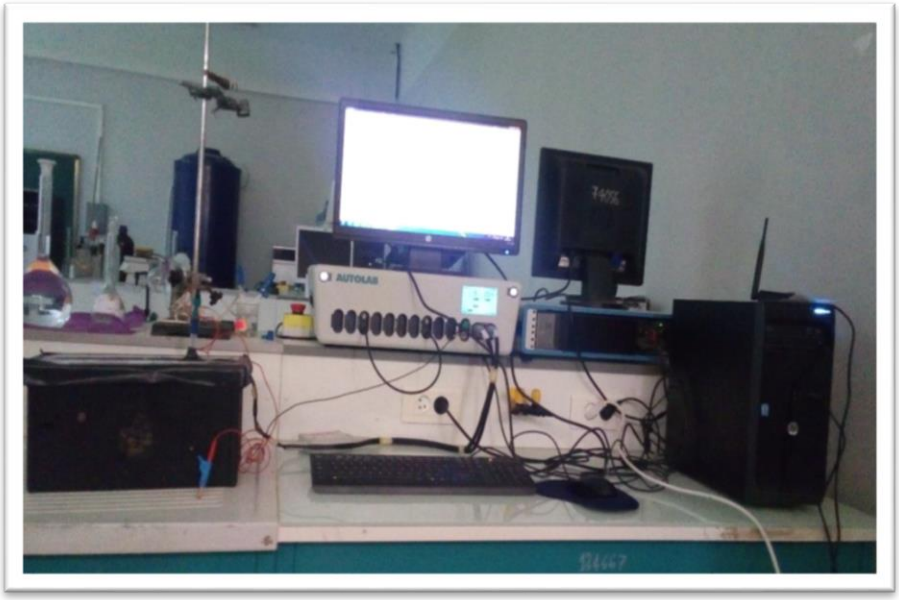

Fig. 3. Schematic representation of the experimental setup.

3.RESULTS AND DISCUSSION

3.1 Photocurrent measurements

Fig. 4 shows the photocurrent variation during 5 consecutive light pulses of 30 seconds each, separated by 3 minutes in the dark. The film was formed potentiostatically at 0.7 V for 2 hours in the dark. It can be seen Upon exposure to light, the current spikes quickly but then decrease just as rapidly, reverting to its initial value in a matter of seconds. This observation confirms the fast electron-hole recombination properties typical of lead oxide. In addition, it can be observed that the current becomes cathodic and that the current intensity is maximal for pure Pb.

Furthermore, it can be seen that the photocurrent $I_{Ph}$of pure Pb increases with the number of pulses, the ones for Pb-0.2% Sn remain unchanged. Whereasfor2% Sn, it decreases with the number of pulses. With each pulse, the photocurrent (I_{Ph}) decreases as the Sn content in the alloy increases from 0 to 2%. This suggests that the addition of Sn introduces energy levels within the band gap that function as electron traps. These energy levels are influenced by the concentration of tin, and as the Sn content rises, the energy levels shift closer to the valence band. At 2% Sn, these levels are most negatively shifted, further reducing the photocurrent.

Another feature (character) was observed (recombination current). When the light is turned off, this oxygen and part of the PbO_n are reduced, which causes a cathode current i_d. At the beginning, this current is i_d°. After As the number of pulses increases, the id° photocurrent decreases after several ignitions of the Pb-Sn electrodes. Figure 4 illustrates that the Sn-containing electrode exhibits a higher photocurrent during the initial pulses than the pure lead electrode. It is evident that Sn speeds up the oxidation of PbO and enhances the electrical conductivity of the PbO_n layer. In the available literature, the decrease in photocurrent has been associated with the formation of an oxygen layer at the PbO_n/solution interface (Pavlov &al, 1977).

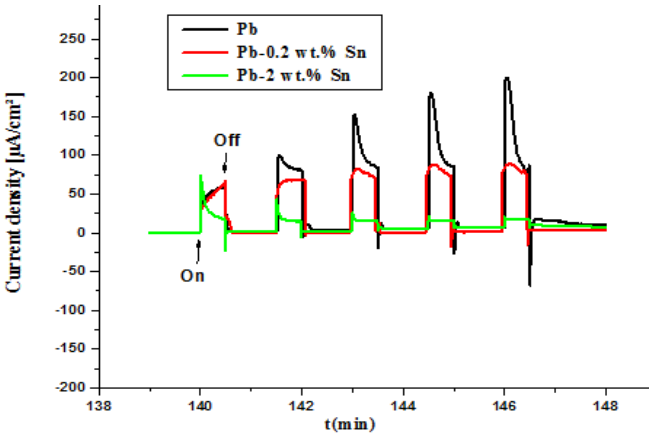

Fig. 4. Photocurrent analysis of passive surface films created on Pb and PbSn at 0.7 V in a 0.5 M solution sulfuric acid for 2 hours

It can be seen that the current increases suddenly when the white light falls on the samples, the current decreases rapidly during the thirty seconds except for the alloys rich in 2% Sn tin. The photocurrent intensity of the pure lead alloy is the highest among the tested alloys and increases progressively with repeated illuminations. In contrast, the photocurrent intensity of the 2% Sn alloy remains consistently low and exhibits minimal variation throughout the series of illuminations.

The initial increase in current upon illumination is primarily attributed to the generation of electron-hole pairs within the semiconductor. The number of electron-hole pairs is significantly higher for pure Pb electrodes. The incorporation of tin into the alloy introduces energy levels above the Fermi level, located between the conduction and valence bands. These energy levels act as electron traps, thereby reducing the photocurrent. As the tin content increases from 0 to 2%, this effect is further amplified due to the formation of more conductive oxides, which enhance the trapping behavior.

At the end of each illumination (30 seconds), a reverse current is produced as a result of the recombination of electron-hole pairs proportional to the number of electron-hole pairs previously created during the previous illumination.

3.2.1 Curves $C_D = f(V)$

Fig. 5 shows the $C_D = f(V)$ curves for each alloy. In addition, it should be noted that as the tin content increases, the potential value of the flat bands decreases.

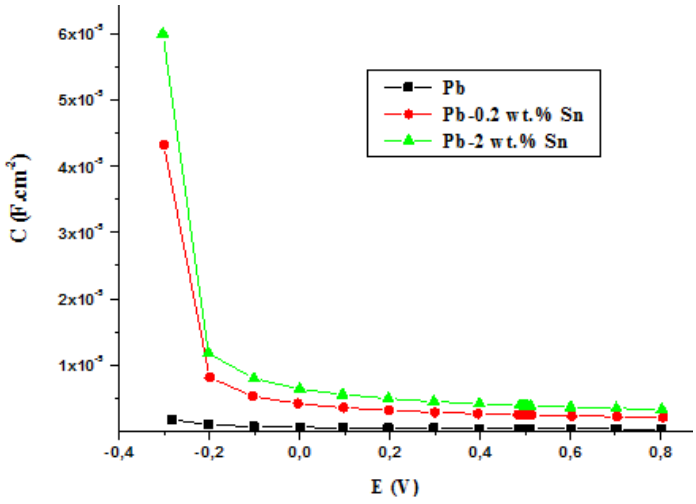

Fig.5. Analysis of the differential capacitance of anodic films generated on Lead and lead-tin alloys at 0.7 V over a 2-hour formation period.

Figure 6 illustrates the variation in the flat band potential as a function of the concentration of electron donor atoms. The resulting curve demonstrates a decreasing trend, and its mathematical representation is as follows:

$$V_{bp} = -0{,}05256 \log N_D + 0{,}57785 \quad (1)$$

It is worth noting that the structure of the semiconductor/electrolyte interface is easier to describe in the case of sufficiently doped semiconductors than in the case of low doping. Indeed, electronic exchanges are much easier at the interface because of the high charge carrier migration in solid and liquid media (J. Schefold, 1992). The potential drop across the Helmholtz layer is primarily dependent on the composition of the electrolyte and is largely unaffected by the space charge region of the semiconductor. When the potential of the semiconductor electrode is altered through the application of an external voltage, the influence remains concentrated on the Helmholtz layer, it alone varies the potential drop across the solid. Consequently, the potential of the flat stripes decreases as the concentration of the electron donor atoms (responsible for the exchange at the interface) increases (Feiner & al, 1987 ;Guyomard, 1986).

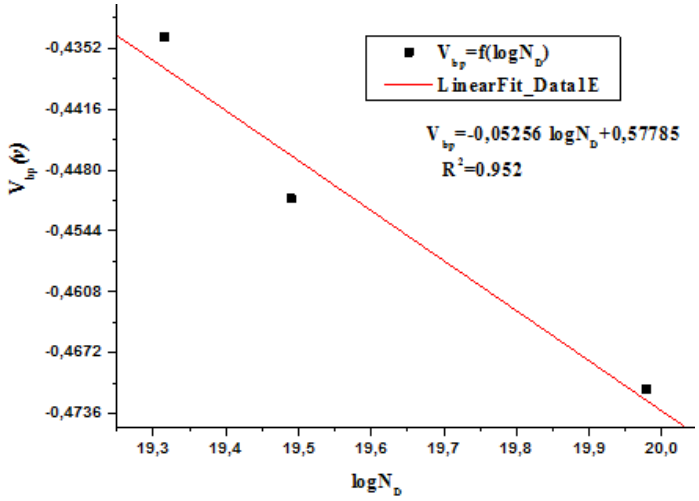

Fig.6. Evolution of V_{bp} as a function of the number of electron donors.

3.2.2 Space charge layer thickness

The space charge layer is an area that forms on the side of the semiconductor when it is brought into contact with an electrolyte. This layer contains the charges associated with the semiconductor, as reported by (Sato, 1998). The thickness of the space charge layer was calculated using the following equation:

$$w_{sc} = \sqrt{\frac{2\varepsilon\varepsilon_0(E - E_{FB})}{eN_D}} \quad (2)$$

Based on the results, it can be observed that the thickness of the space charge layer increases as the concentration of mobile charge carriers decreases. This observation is consistent with findings reported by (1998). The values for the thickness of the space charge layer are presented in Table 1.

Table 1. Refined measurements of space-charge layer thickness W_{SC}

Alloys	The space charge layer's thickness W_{SC} (μm)
Pb	0.919
Pb alloy with 0.2 wt.% tin	0.810
Pb alloy with 2 wt.% tin	0.465

3.3 Analysis of Data from Electrochemical Impedance Spectroscopy

Fig.7 shows the results obtained at the Nyquist level. At a voltage of 0.7 V, the resistance of the wear layers formed on different alloys was measured to understand the mechanism of sulfate and α-PbO formation. Furthermore, the resistance was measured again at different polarization potentials: 0.2 V, 0.4 V, 0.6 V and 0.7 V, respectively. According to results, For all samples, the arc of the impedance loop (representing corrosion resistance) increases with the applied potential at 0.2 V, 0.4 V, 0.6 V, and 0.7 V, respectively. This increase is attributed to the growing formation of $PbSO_4$ and PbO, which significantly enhance the corrosion layer's resistance, particularly when the substrate is pure and the potential is close to 0.7 V. Additionally, it is observed that at 0.7 V, the polarization resistance decreases as the tin content increases in all alloys.

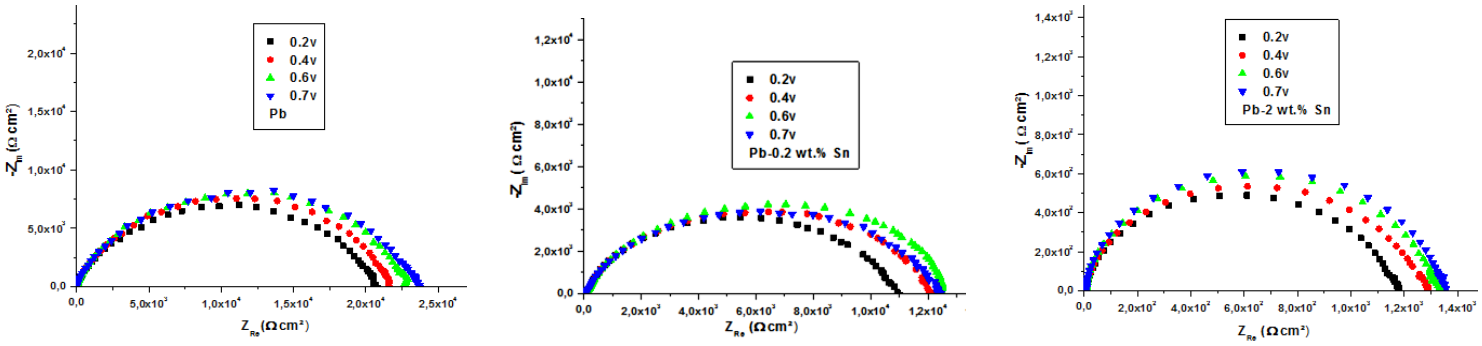

Fig. 7. Nyquist representations of the experimental results for anodic layers on Lead and lead-tin alloysat 0.2, 0.4, 0.6, and 0.7 V in a 0.5 M sulfuric acid solution at 25°C.

The EIS results further support these findings, showing that the corrosion resistance of PbO improves with increasing tin content. The Nyquist plots demonstrate a clear increase in the arc of the corrosion loop with applied potentials, indicating improved stability of the PbO layer, especially at higher tin concentrations. This enhanced stability makes PbO an excellent candidate for use in renewable energy applications where long-term durability is essential, such as in PECs and solar cells.

3.4 Tafel polarization results

The Tafel plots (Fig. 8) were generated using a linear voltammetry procedure by scanning the working electrode potentials from -1 V to 0.7 V relative to the saturated $Hg/Hg_2SO_4/K_2SO_4$ reference electrode, at a scan rate of 10 mV/s, in a 0.5 M sulfuric acid solution at 25°C. Table 2 presents the corrosion current density values as a function of the tin content in the alloy, providing insights into the wear resistance of the PbSn alloy. We can clearly notice that tin reduces the corrosion resistance, in other words, tin reduces the polarization resistance of tin-lead alloys. The same finding was made in the EIS results.

Table 2 shows the parameters extracted from the Tafel curves obtained.

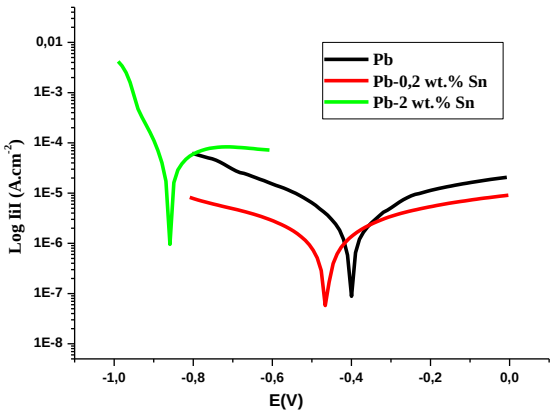

Fig. 8. Tafel polarization curves of films created on Lead and lead-tin alloys anodically at 0.7 V for 2h.

From Fig. 8 above and Table 3, we can deduce that the corrosion current of the tin-rich alloy is higher than that of the Pb-0% Sn and Pb-0.2% Sn alloys. Among the tested alloys, the Pb-0.2% Sn alloy exhibits the lowest corrosion current. This can be explained by the thickness of the layer formed. In this alloy (Pb-2% Sn), we have shown that tin reduces this thickness and thus reduces the amount of $PbSO_4$ formed. This increases the conductivity of the layer formed. The polarisation resistance of tin-rich alloys is reciprocally minimal.

Another point to note concerns the corrosion potential. This shifts cathodically as the tin content increases. This can be explained by the fact that the standard potential of tin (-0.136 V/ENH) is lower than that of lead (-0.126 V/ENH). The tin especially segregated in the grain boundaries of the oxides beforehand giving different oxides with different conductivities.

Table 2. Polarization parameter values of films created on Lead and lead-tin alloys anodically at 0.7 V for 2h

Alloys	**b_a (V/dec)**	**b_c (V/dec)**	**$E_{corr}(V)$**	**$i_{corr}(A)$**	Polarization resistance (Ω)
Pb	0.49515	0.82128	-0.42269	7.959E-6	16856
Pb alloy with 0.2 wt.% tin	0.5641	0.52887	-0.46303	2.1894E-6	54145
Pb alloy with 2 wt.% tin	0.085247	0.4594	-0.85916	5.2512E-5	594.67

The Tafel polarization curves indicate that, while increasing the tin content reduces the corrosion resistance of the alloy, this reduction is offset by the formation of more conductive oxides, which enhance the overall conductivity of the corrosion layer, resulting in enhanced photoelectrochemical activity. This trade-off between corrosion resistance and electrical conductivity is critical for optimizing PbO's performance in energy conversion devices.

3.5 XRD results

Fig.9 shows the results of the X-ray diffraction test of films created on Lead and lead-tin alloys anodically at 0.7 V in 0.5 M sulphuric acid at 25°C for 2 hours. The results show the presence of $PbSO_4$, PbO and Pb; the X-rays penetrate the film because the anodic layer is very thin, and the Pb layer is shown in spectroscopy. Several peaks also appear. By comparing the peak intensities and the average distances between the peak levels for the different alloys, using a JCPDS map (version 2.02, 1999), the structural and compositional variations across the alloys can be analyzed effectively, it can be seen that they are quite close together. The effect of tin in the reduction of sulphate and lead monoxide in the wear layer can also be noted. Table 3 summarizes the most important results of X-ray diffraction (XRD) from d_{hkl} crystal distance and hkl

directions. The values with a dark black color are taken from the PCPDFWIN database (JCPDS, v. 2.02, 1999).

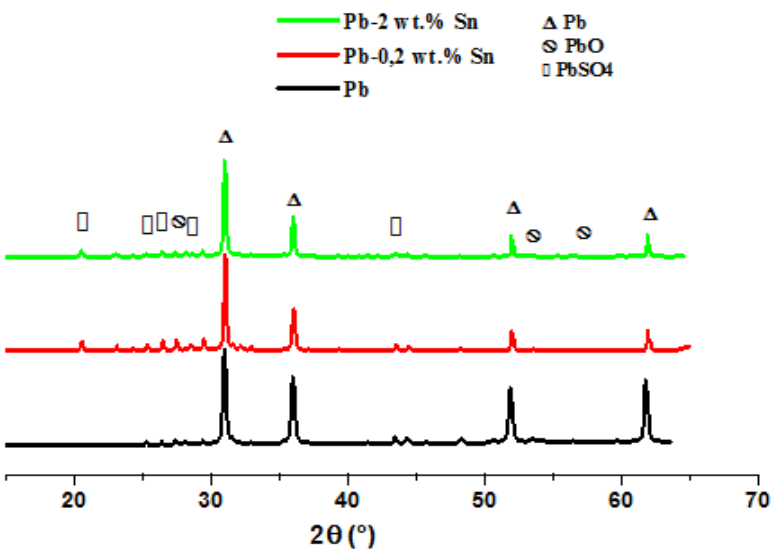

Fig.9. XRD patterns of films created on Lead and lead-tin alloys anodicallyat 0.7V in 0.5MH_2SO_4 at 25°C.

Table 3. Summary of results obtained from XRD of films created on Lead and lead-tin alloys anodicallyat 0.7V in 0.5MH_2SO_4 at 25°C.

	d_1(hkl)	d_2(hkl)	d_3(hkl)	d_4(hkl)	d_5(hkl)
Pb	2.77018 (111) **2.84634**	2.40964 (002) **2.46500**	1.72219 (022) **1.74302**	1.47242 (113) **1.48645**	
PbO	3.10497 (111) **3.10370**	1.67559 (311) **1.67100**	1.59656 (222) **1.55180**		
$PbSO_4$	4.21076 (020) **4.23792**	3.35052 (021) **3.33449**	3.21590 (210) **3.21902**	3.03577 (121) **3.00519**	2.11402 (040) **2.11807**

3.6 SEM results

Scanning Electron Microscopy (SEM) provides detailed insight into the surface morphology of the samples. SEM images of the oxide films formed on Lead and lead-tin alloys after 2 hours of immersion in a 0.5 M sulfuric acid solution reveal distinct differences in surface structure. As shown in Fig. 10, the lead electrode develops a fine crystalline film, whereas the surface of the tin alloy exhibits coarser crystal structures. These morphological differences suggest that the addition of tin influences the formation and growth of oxide layers, leading to more pronounced, larger crystalline structures on the PbSn alloy, which may increase the porosity of the film; this leads us to conclude that tin has an effect in the form of PbO and $PbSO_4$ crystals.

In Pb-0.2% Sn alloys, we see large, finely interconnected prismatic crystals of $PbSO_4$. Small round crystals, also known as rock-like crystals, can also be observed. The $PbSO_4$ crystals in the layer obtained on pure lead are superficially etched. It should be noted that the PbO under the $PbSO_4$ membrane is unstable in this type of electrolyte and spontaneously transforms into lead sulphate. Tin in excess of 0.2% thins the resulting layer, reducing the $PbSO_4$ content.

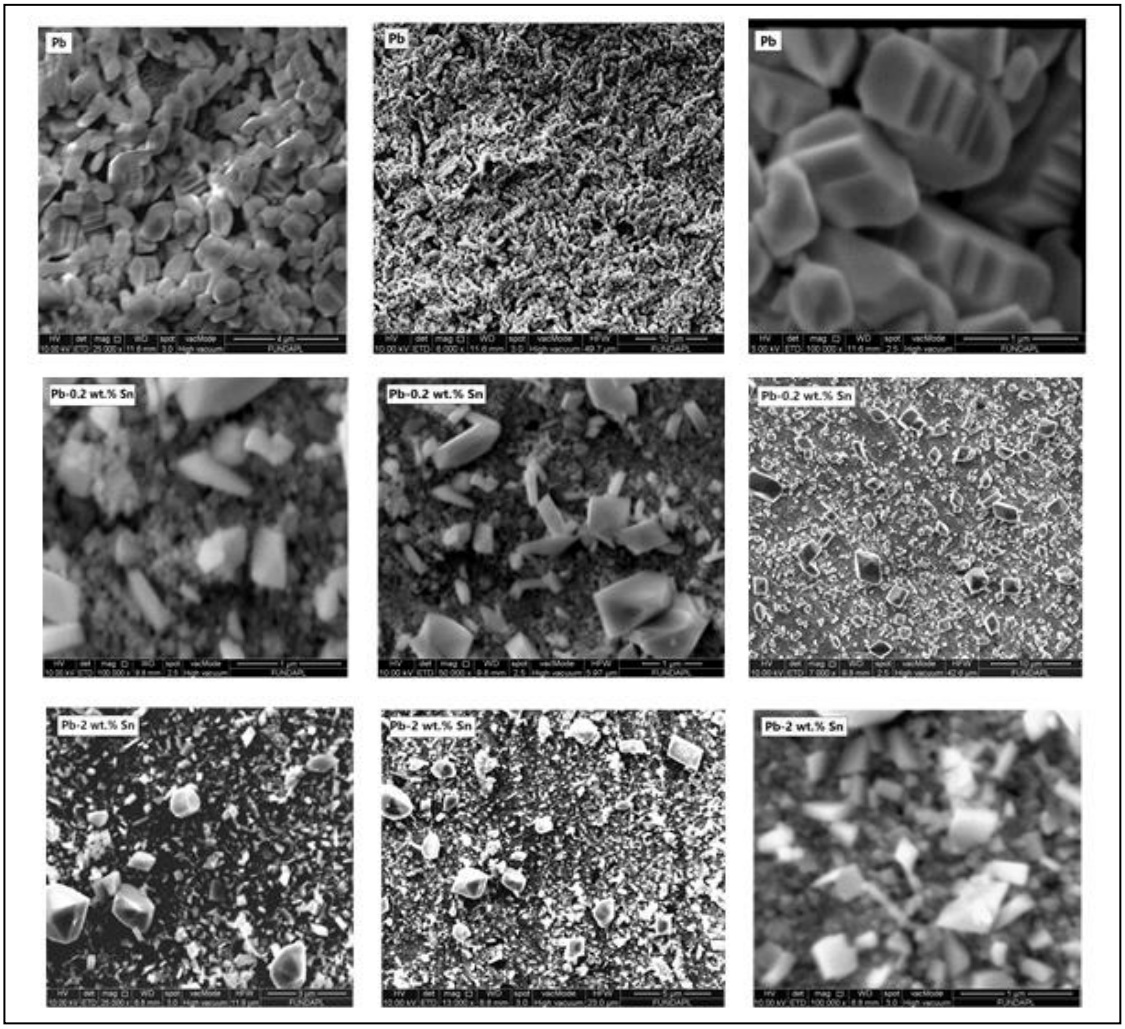

Fig. 10. SEM analysis of oxide films produced on Lead and lead-tin alloys at 0.7 V in 0.5 M H_2SO_4 at 25°C

4. CONCLUSION

This study focused on investigating the impact of the substrate on the photoelectrochemical and semiconductive properties of lead oxide in a 0.5 M H_2SO_4 solution at 0.7 V, compared to a $Hg/Hg_2SO_4/K_2SO_4$ saturated electrode for 2 hours. Through various analytical techniques, it was observed that the addition of tin reduces the thickness of the corrosion layer while enhancing its conductivity by forming conductive and photoactive tin oxides, as well as a dense layer between the grid and the positive active mass. Moreover, a strong correlation between the results obtained from Electrochemical Impedance Spectroscopy (EIS) and Tafel polarization methods was noted. The modifications to lead oxide substrates, particularly with tin incorporation, offer substantial improvements in renewable energy applications by enhancing the efficiency and durability of energy storage systems. These advancements contribute to more efficient energy conversion technologies and further support environmental sustainability efforts.

ACKNOWLEDGEMENTS

We would like to thank the head of the inorganic chemistry laboratory at the University of M'sila for his assistance in carrying out this research work**.**

REFERENCES

Barradas, R.G., Nadezhdin, D.S., Webb, J.B., Roth, A.P., Williams D.F. (1981). Some photoelectrochemical observations on lead under anodic oxidation in sulphuric acid. J. Electroanal. Chem., 126(1–3), 273–276. https://doi.org/10.1016/S0022-0728(81)80434-2

Buchanan, J. S., & Peter, L. M. (1988). Photocurrent spectroscopy of the lead electrode in sulphuric acid. Electrochimica Acta, 33(1), 127–136. https://doi.org/10.1016/0013-4686(88)80044-6

Bullock, K. R., Trischan, G. M., & Burrow, R. G. (1983). Photoelectrochernical and Microprobe Laser Raman Studies of Lead Corrosion in Sulfuric Acid. J. EIectrochem. Soc.: Electrochenical Science and Technology, 130(6), 1283–1289. https://doi.org/https://doi.org/10.1149/1.2119939

Campbell, S. A., & Peter, L. M. (1991). A photoelectrochemical study of the reduction of electrodeposited α-PbO2in ethanoate solution. Journal of Electroanalytical Chemistry. https://doi.org/10.1016/0022-0728(91)87014-U

Carter, B.J., Stefano, S.D., Whitcanack, L. (1986). Ext. Abstr. The Electrochemical Society, Pennington, NJ, USA. Ext. Abst. No. 94, Vol. 86-2, 133.

Cimek, J., Stępień, R., Klimczak, M., Zalewska, I., Buczyński R. (2017). Development of thermally stable glass from SiO2-Bi2O3-PbO-ZnO-BaO oxide system suitable for all-solid photonic crystal fibers. Optical Materials, 73, 277–283. https://doi.org/10.1016/J.OPTMAT.2017.08.028

El-Mallawany, R., Sayyed, M. I., Dong, M. G., & Rammah, Y. S. (2018). Simulation of radiation shielding properties of glasses contain PbO. Radiation Physics and Chemistry, 151, 239–252. https://doi.org/10.1016/J.RADPHYSCHEM.2018.06.035

Feiner, A.S., McEvoy, A.J., Infelta, P.P. (1987). Crystal-face specific electrochemical effects on cadmium sulphide. Science, Surface, 189, 411–419. https://doi.org/10.1016/S0039-6028(87)80461-2

Guyomard, D. (1986). Mise au Principes de base de l'électrochimie des semi-conducteurs. J. Chim. Phys.,83, 355–391. https://doi.org/https://doi.org/10.1051/jcp/1986830355

Shao-you, L., Yuan-dao, C., Tao-yu, Q. et al. (2018). Sulfur Doped Lead Monoxide Superfine Powder Materials: Solid-State Synthesis, Characterization, Adsorption and Photocatalytic Property of Methylene Blue. Journal of Inorganic and Organometallic Polymers and Materials, 28, 2584–2595. https://doi.org/10.1007/s10904-018-0942-4

Liu, W., Ma, B., Fu, Y., Zhang, K., Mezaal, M. A., Li, F., Zhao, X., & Lei, L. (2017). Electrochemical property of α-PbO prepared from the spent negative powders of lead acid batteries. Journal of Solid State Electrochemistry. https://doi.org/10.1007/s10008-016-3333-1

Mohamed E & al. (2018). Recycled high-density polyethylene plastics added with lead oxide nanoparticles as sustainable radiation shielding materials. Journal of Cleaner Production, 176, 276–287. https://doi.org/10.1016/j.jclepro.2017.12.100

Nelson, R. F., & Wisdom, D. M. (1991). Pure lead and the tin effect in deep-cycling lead/acid battery applications. Journal of Power Sources, 33(1–4), 165–185. https://doi.org/10.1016/0378-7753(91)85058-5

Patel, D. B. and Mukhopadhyay, I. (2015). Schottky junction solar cells based on nonstoichiometric PbOx film. Journal of Physics D: Applied Physics, 48, 025102. https://doi.org/10.1088/0022-3727/48/2/025102

Pavlov, D., Bashtavelova, E., Iliev, V. (1984). Structure of the lead-acid battery active masses. In Proceedings of the Symposium on Advances in Lead-Acid Batteries. Proceedings of the Symposium on Advances in Lead-Acid Batteries, 16.

Pavlov, D. (1978). Processes in solid state at anodic oxidation of a lead electrode in H2SO4solution and their dependence on the oxide structure and properties. Electrochimica Acta, 23, 845–854. https://doi.org/10.1016/0013-4686(78)87005-4

Pavlov, D. (1981). Semiconductor mechanism of the processes during electrochemical oxidation of PbO to PbO2. Journal of Electroanalytical Chemistry, 118, 167–185. https://doi.org/10.1016/S0022-0728(81)80539-6

Pavlov, D., Poulieff, C.N., Klaja, E. and Iordanov, N. (1969). Dependence of the Composition of the Anodic Layer on the Oxidation Potential of Lead in Sulfuric Acid. Journal of The Electrochemical Society, 116(3), 316–319. https://doi.org/https://doi.org/10.1149/1.2411836

Pavlov, D., Zanova, S. and Papazov, G. (1977). Photoelectrochemical Properties of the Lead Electrode during Anodic Oxidation in Sulfuric Acid Solution. J. Electrochem. See: Electrochemical Science and Technology, 124(10), 1522–1528. https://doi.org/10.1149/1.2133105

Pendry, C. (1999). how-compressible-is-recombinant-battery-separator-mat. Journal of Power Sources, 78(1–2), 54–64. https://doi.org/https://doi.org/10.1016/S0378-7753(99)00011-7

Peter, L. M. (1983). A photoelectrochemical study of the reduction of alpha lead dioxide in aqueous sodium tetraborate. J. Electroanal. Chem, 144, 315–330. https://doi.org/https://doi.org/10.1016/S0022-0728(83)80164-8

Foroughi, M.M. and Ranjbar, M. (2017). Graphene Oxide Doped with PbO Nanoparticles, Synthesis by Microwave Assistant Thermal Decomposition and Investigation of Optical Property. Journal of Cluster Science, 28, 2847–2856. https://doi.org/10.1007/s10876-017-1248-3

Rocca, E., & Steinmetz, J. (1999). Mechanism of passivation of Pb(Ca)-Sn alloys in sulfuric acid: Role of tin. J Electrochimica Acta, 44, 4611–4618. https://doi.org/10.1016/S0013-4686(99)00186-3

Sato, N. (1998). Electrochemistry at Metal and Semiconductor Electrodes. Elsevier. https://doi.org/10.1016/B978-0-444-82806-4.X5000-4

Schefold, J. (1992). Flatband Potentials, Barrier Heights, and Charge Transfer at the n-lnP/Electrolyte Contact. Journal of The Electrochemical Society, 139, 2862–2871. https://doi.org/10.1149/1.2068993

Semeniuk, O., Grynko, O., Juska, G. et al. (2017). Amorphous lead oxide (a-PbO): suppression of signal lag via engineering of the layer structure. Scientific Reports, 7(1), 1–7. https://doi.org/10.1038/s41598-017-13697-2

Srivastava, J. K., Pandey, P., Mishra, V. N., & Dwivedi, R. (2011). Structural and micro structural studies of PbO-doped SnO2 sensor for detection of methanol, propanol and acetone. In Journal of Natural Gas Chemistry, 20(2), 179–183. https://doi.org/10.1016/S1003-9953(10)60168-5

Weininger, J. L., & Siwek, E. G. (1976). Corrosion of Lead Alloys at High Anodic Potentials. Journal of The Electrochemical Society, 123(5), 602–606. https://doi.org/10.1149/1.2132893

Zentai, G., Partain, L.D., Pavlyuchkova, R. et al. (2013). Mercuric Iodide and Lead Iodide X-Ray Detectors for Radiographic and Fluoroscopic Medical Imaging. Proc. SPIE 5030, Medical Imaging 2003: Physics of Medical Imaging, 77–91. https://doi.org/10.1117/12.480227

Zheng, C., Li, W., Chen, W., Ye, X., Cai, S. and Xiao, X. (2014). Microstructure and optical limiting properties of multicomponent inorganic gel-glasses: A focus on SiO2, TiO2 and PbO gel-glasses. Ceramics International, 40(2), 2669–2675. https://doi.org/10.1016/j.ceramint.2013.10.057

Zhuravlev, Y. N., & Korabel'nikov, D. V. (2017). A First Principles Study of the Mechanical, Electronic, and Vibrational Properties of Lead Oxide. Original Russian Text © Yu.N. Zhuravlev, 59(11), 2272–2286. https://doi.org/10.1134/S106378341711035X